A mix design methodology of slag and fly ash-based alkali-activated paste

Sun, Beibei ; Sun, Yubo; Ye, Guang; De Schutter, Geert

DOI
10.1016/j.cemconcomp.2021.104368

Publication date
2022

Document Version
Final published version

Published in
Cement and Concrete Composites

Cement and Concrete Composites 126 (2022) 104368

Contents lists available at ScienceDirect

Cement and Concrete Composites

journal homepage: www.elsevier.com/locate/cemconcomp

A mix design methodology of slag and fly ash-based alkali-activated paste

Beibei Sun [a], Yubo Sun [a], Guang Ye [a,b,**], Geert De Schutter [a,*]

[a] Ghent University, Department of Structural Engineering and Building Materials, Magnel-Vandepitte Laboratory, Technologiepark-Zwijnaarde 60, 9052, Ghent, Belgium
[b] Microlab, Section Materials and Environment, Faculty of Civil Engineering and Geosciences, Delft University of Technology, Stevinweg 1, 2628, CN, Delft, the Netherlands

ARTICLE INFO

Keywords:
Slag and fly ash-based alkali-activated materials
Control factors
Flowability
Setting time
Strength
Mix design

ABSTRACT

In this paper, a series of experiments were conducted to systematically and quantitively explore the effects of control factors on the early age properties, i.e., workability and strength of slag and fly ash-based alkali-activated paste (BFS/FA-AAP). The control factors on the workability (flowability and setting time) of BFS/FA-AAP include the Na_2O/b ratio, the SiO_2/Na_2O ratio, the w/b ratio, and the BFS/b ratio. The control factors on strength (compressive strength and flexural strength) of BFS/FA-AAP further also include the curing condition and the curing age. The results show that a higher BFS/b ratio and Na_2O/b ratio could increase the strength while decreasing the workability. A higher w/b ratio could increase the workability while slightly decreasing the strength. Higher SiO_2/Na_2O ratio increases both strength and workability. Despite that, higher Na_2O/b ratio and SiO_2/Na_2O ratio could hinder the strength development. Sealed curing condition is proved to be a simple but efficient way to assure the steady strength development of BFS/FA-AAP. Although the strength of BFS/FA-AAP could generally stabilize after 90 days, the strength development rate varies with different mix proportions. In addition, a general methodology have been proposed to predict the compressive strength of BFS/FA-AAP and verified with experiments. Finally, a mix design table is proposed for the preliminary design of BFS/FA-AAP according to the principle of satisfying early age requirements.

1. Introduction

The application of alkali-activated materials as an alternative to cement-based materials has substantial economic and environmental benefits because it can reduce not only CO_2 emission but also industry waste disposal [1–4]. Previous researches have shown that a good overall performance could be achieved when alkali-activated material is made by blast furnace slag (BFS) and fly ash (FA), sodium hydroxide, and sodium silicate [5–11]. Compared with cement-based material, slag and fly ash-based alkali-activated materials (BFS/FA-AAM) has lots of advantages, such as rapid strength gaining, low thermal conductivity, high volume stability, fire resistance, and chemical erosion resistance. Recently, BFS/FA-AAM has received more and more attention from the academic field. A large number of researchers studied its fresh and hardened properties.

The workability of the BFS/FA-AAM has a direct influence on pumping and processing. Nedeljkovic et al. [12] reported that BFS/FA-AAM with a higher FA content enables an enhancement in workability. Deb et al. [9] found that the decrease of alkali solution to binder ratio from 0.4 to 0.35 reduces the workability. The research of Oderji et al. [13] shows that when sodium silicate content is 8%, the workability of BFS/FA-AAM is optimal. Vikas et al. [14] pointed out that BFS/FA-AAM with the molarity of sodium silicate larger than 2.85 could achieve better workability compared to that with a molarity of 1.99. Fang et al. [15] reported that the workability of BFS/FA-AAM decreases with an increase of sodium hydroxide molarity.

Appropriate setting time of BFS/FA-AAM is of great importance since it affects the transportation, pouring process, and construction speed. The study of Humad et al. [16] proved that BFS/FA-AAM with high FA content is successful in delaying the setting times. Fang et al. [15] found that a higher alkali solution to binder ratio prolongs the setting time of BFS/FA-AAM. Samantasinghar and Singh [17] reported that the setting times of BFS/FA-AAM drop rapidly with the concentration of sodium hydroxide from 2 M to 16 M. Vikas et al. [14] reported that the setting time of BFS/FA-AAM increases with the molarity of sodium silicate (from 1.99 to 2.85). Ouyang et al. [18] pointed out that when the

* Corresponding author.
** Corresponding author. Ghent University, Department of Structural Engineering and Building Materials, Magnel-Vandepitte Laboratory, Technologiepark-Zwijnaarde 60, 9052, Ghent, Belgium.
E-mail addresses: g.ye@tudelft.nl (G. Ye), Geert.DeSchutter@ugent.be (G. De Schutter).

https://doi.org/10.1016/j.cemconcomp.2021.104368
Received 27 October 2021; Received in revised form 26 November 2021; Accepted 29 November 2021
Available online 1 December 2021

activator modulus changes, the influence of BFS content on the setting time and workability of BFS/FA-AAM presents different trends.

Strength is the most valuable characteristic of BFS/FA-AAM as a building material. Sajjad et al. [13] reported that the compressive strength of BFS/FA-AAM could be improved by increasing BFS content. According to the study of Oderji et l. [13], the optimum concentration of sodium silicate is 8% with consideration of compressive strength. The optimum molarity of sodium silicate is found to be 1 in the study of Ouyang et al. [18]. Fang et al. [15] found that the compressive strength of BFS/FA-AAM increased with the decrease of alkali solution to binder ratio, as well as the increase of molarity of sodium hydroxide. Similarly, the research of Saha and Rajasekaran [19] shows that the compressive strength of BFS/FA-AAM increases with the increase of sodium hydroxide concentration from 6 M to 16 M. Nevertheless, some researchers report that there is an optimum value of sodium hydroxide concentration. For example, the result of Samantasinghar and Singh [17] indicates that the optimum value of sodium hydroxide concentration is 8 M, while the research of Singh et al. [20] shows that the optimum value is 14 M. Rashad et al. [21] indicated that the tendency of flexural strength development and compressive strength development in BFS/FA-alkali activated mortar is similar, which are both influenced by the ratio of fly ash and slag. Chi et al. [22] further proved it and found that the flexural strength of BFS/FA-alkali activated mortar could be influenced by the dosage of Na_2O. The results of Fang et al. [15] revealed that a higher molar ratio of sodium silicate could improve the flexural strength of BFS/FA-alkali activated mortar, while the sodium hydroxide to sodium silicate ratio does not influence it. Nath et al. [23] conducted experiments and obtained the relationship between the flexural strength and the compressive strength of BFS/FA-alkali activated concrete by fitting the experimental data ($f_{ct,f} = 0.93\sqrt{f_c}$).

All these researches have provided insights on how different influencing factors affect the properties of the BFS/FA-AAM. Although extensive research has been carried out, no single study exists which systematically studies all the influencing factors on BFS/FA-AAM. Due to the complexity of the system, there is not yet an unified definition of influencing factors. For example, the molar ratio of sodium silicate and the concentration of sodium hydroxide vary from different sources which leads to a vague sodium silicate to sodium hydroxide ratio. Using the alkali activator to binder ratio could lead to inconsistent results because the reaction components and water in the activator have the opposite effect. Nevertheless, the definition of the water to binder ratio is different from the literature since water exists not only in additional tap water but also in sodium hydroxide and sodium silicate solution. Previously published studies on the effect of some factors are not consistent. Because a combined effect exists, solely discussing the influence of a factor without considering the difference in other components might lead to completely different conclusions.

The unclear definition of influencing factors and inconsistent results further causes difficulties in forming an unified mix design method of BFS/FA-AAM. Existing literatures have put forward some mix proportions with good performance, most of which are based on extensive experimental screening [24–30]. The mixtures are difficult to replicate because not all the essential parameters are considered in the mix design procedure, or the studies failed to give detailed design steps, and are limited to specific experimental conditions [31]. Currently, the application of FA/BFS-AAM has been mostly restricted by the lack of a mix design methodology. The urgent task of popularizing BFS/FA-AAM is to put forward a suitable, practical, and straightforward mix design method.

Unlike cement material, the composition of BFS/FA-AAM is more complex. It is more meaningful to study the mix proportion from the perspective of chemical composition (control factors) rather than the perspective of raw material content. Therefore, 5 most representative factors are selected in this research as control factors of early properties of BFS/FA-AAM which include the Na_2O/b ratio, the SiO_2/Na_2O ratio, the w/b ratio, the BFS/b ratio, and the curing age. It is known that cement paste plays a decisive role in the compressive strength and setting time of ordinary portland cement concrete. Likewise, the performance of alkali-activated paste determines the compressive strength and setting time of the alkali-activated concrete. Moreover, it is worth noting that the workability of alkali-activated concrete depends not only on water content but also on the proportion of other components in the paste. Previous researches have shown that the workability of alkali-activated concrete could change greatly with different mix proportion of its paste [15,21,32,33]. Therefore, the workability of paste could be an important indicator for designing the flowability of alkali-activated concrete. The main purpose of this study is to understand how the control factors influence the fresh and hardened properties of slag and fly ash-based alkali-activated paste (BFS/FA-AAP). Another goal of this paper is to establish evaluation methods for early age properties i.e., flowability, setting time, strength of BFS/FA-AAP according to the mix proportion, and to build a mix design method of BFS/FA-AAP according to the requirements of early age properties.

2. Experimental procedure

2.1. Materials

BFS from ECOCEM (Moerdijk, The Netherlands) and class F FA from VLIEGASUNIE (Amsterdam, The Netherlands) were used as precursors to prepare the BFS/FA-AAP in this study. BFS has a specific gravity of 2890 kg/m^3 and a 100% vitreous phase content, while FA has a specific gravity of 2300 kg/m^3 and a vitreous phase content of 68%. The chemical composition of the precursor determined by X-ray fluorescence (XRF) is listed in Table 1. The basicity coefficient (Kb=(CaO + MgO)/(SiO_2+Al_2O_3)) of BFS is 0.95, and the quality coefficient (HM=(CaO + MgO + Al_2O_3)/SiO_2) of BFS is 1.6, indicating that this BFS has high reactivity [34,35]. The aluminum saturation index (ASI = Al_2O_3/(Na_2O + K_2O+2CaO)) of FA is 2.55, which represents that Al acts as both network former and network modifier [36,37]. The particle distribution of BFS and FA is detected by laser diffraction using a particle analyzer Malvern Mastersizer 2000 E (See Fig. 1). The average particle sizes (D50) of BFS and FA are 8.5 μm and 8.3 μm, respectively. The morphology of BFS and FA particles is observed by a scanning electron microscope (SEM) 505 Philips (see Fig. 2). BFS particles are irregular while FA particles consist of spheres, cenospheres, and pherospheres [38].

The activators used in this study are sodium silicate and sodium hydroxide, both of which are from BRENNTAG (Deerlijk, Belgium). The chemical composition of sodium silicate solution is 27.5 wt% SiO_2, 8.25 wt% Na_2O, and 64.25 wt% H_2O. The sodium hydroxide used in this

Table 1
Chemical composition of BFS and FA measured by XRF (wt%).

Element	BFS	FA
SiO_2	31.1	56.7
CaO	40.9	3.74
Al_2O_3	13.7	24
MgO	9.16	1.75
Fe_2O_3	0.401	2.3
MnO	0.31	0.0579
CuO	0.0054	0.0149
Rb	0.0032	0.0109
SO_3	2.31	1.04
ZrO_2	0.119	0.103
SrO	0.0741	0.129
Ti_2O	1.26	1.16
As	0.0006	0.0071
ZnO	0.003	0.0238
K_2O	0.685	–
Na_2O	–	1.94
Other components	0	7.0234

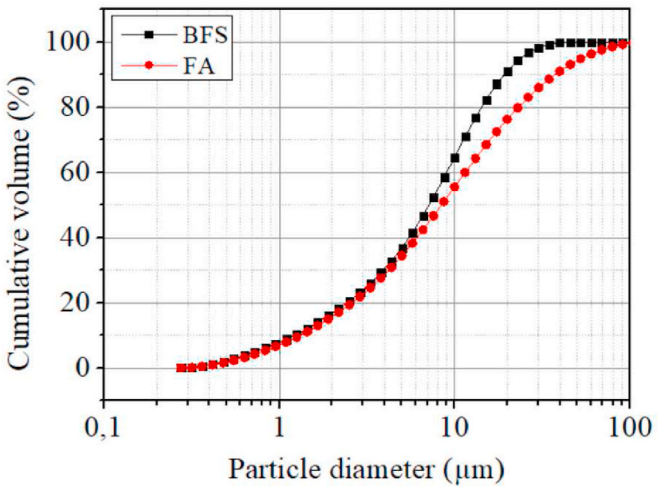

Fig. 1. Particle size distributions of BFS and FA.

study is hygroscopic pearls with 99% of NaOH. The final activators were prepared by pre-dissolving sodium hydroxide in sodium silicate and tap water according to the mix proportion a day before casting.

2.2. Mixture proportions and mixing protocols

Two experiments were designed to comprehensively investigate how the control factors influence the early age properties of BFS/FA-AAP. The control factors and levels considered are listed in Table 2. All ratios in the table are mass ratios. "w" refers to the sum of water from both activators and additional tap water. "b" refers to the sum of BFS and FA. "Na_2O" refers to the sum of Na_2O in the activator from both sodium hydroxide and sodium silicate. "SiO_2" refers to silica equivalent in sodium silicate activator.

Specifically, experiment 1 is for studying the effect of Na_2O/b, SiO_2/Na_2O ratio on the flowability, setting time, flexural strength, and compressive strength of BFS/FA alkali-activated materials. Experiment 1 also studies the effect of curing conditions on flexural and compressive strength of BFS/FA alkali-activated materials. The BFS/b ratio of 0.5 and the w/b of 0.4, as the most commonly used parameters in the research of BFS/FA-AAM, were used in experiment 1. For comparison, 2 sets of the specimen with the same mix proportion were cured in different conditions: the standard condition (>95% relative humidity, 20 ± 2 °C) and sealed condition (sealed 2 layers with plastic wrap, 20 ± 2 °C) till the testing day(1 d, 7 d, 28 d, 56 d, 90 d). Experiment 2 is for investigating the effect of the BFS/b ratio and the w/b ratio on the flowability, setting time, flexural strength, and compressive strength of BFS/FA alkali-activated materials. The Na_2O/b ratio and the SiO_2/Na_2O ratio are 5% and 1.5, respectively. The parameters are most frequently used in the research of BFS/FA-AAM. All specimens were cured at the sealed condition till the testing day (1 d, 7 d, 28 d, 56 d, 90 d).

According to Table 2, the BFS/FA-AAP mixtures were prepared in a Hobart mixer by the following procedure: 1) All solid materials were premixed for 2 min at a mixing speed of 140 rpm; 2) The alkali-activated solution was then added and mixed for 1min at 140 rpm; 3) The layer of material sticking to the mixing arm, the walls, and bottom of the mixing bowl was scraped and recollected during the 30 s of rest. 4) The mix continued to be mixed at 285 rpm for 1 min 30 s.

2.3. Testing program

From the addition of activator till 5 min, 15 min, 30 min, 45 min, 60 min, the flowability of BFS/FA-AAP was measured at each time point by a mini-slump test [12] according to the following steps: 1) The fresh mixture was poured into a slump cone (a top inner diameter of 38 mm, a bottom inner diameter of 62 mm, and a height of 40 mm) that was placed in the center of a flow table; 2) The cone was lifted and the diameters of the subsided mixture were measured in two vertical directions. The average value is recorded as flowability.

The initial and final setting times of BFS/FA-AAP were measured by an automatic recording Vicat needle apparatus according to BS EN 196–3:2016. The setting time tests were conducted at 20 °C and 60% relative humidity. Starting from the moment of adding alkali-activated solution, the time at which the test needle of the apparatus sinks 6 ± 3 mm from the bottom plate was recorded as the initial setting time, and the time at which the test needle sinks into the BFS/FA-AAP no more than 0.5 mm was recorded as the final setting time.

The compressive strength and flexural strength of BFS/FA-AAM were tested according to EN 12390-4-2000. After proper mixing, the mixtures were cast in molds (40 × 40 × 160 mm^3) and immediately covered with a plastic layer to avoid evaporation of water. All specimens were stored in a room with a temperature of 20 °C and relative humidity of 60%. The specimens were demolded after 1 day, then cured at the curing conditions mentioned above till the testing day. The flexural strength is measured by a three-point bending test. The two halves of the specimens

Table 2
Factors and levels considered.

Factors	Levels (experiment 1)	Levels (experiment 2)
Na_2O/b	2%; 4%; 6%; 8%; 10%	5%
SiO_2/Na_2O	0; 0.5; 1; 1.5; 2	1.5
BFS/b	0.5	0; 0.25; 0.5; 0.75; 1
w/b	0.4	0.3; 0.35; 0.4; 0.45; 0.5

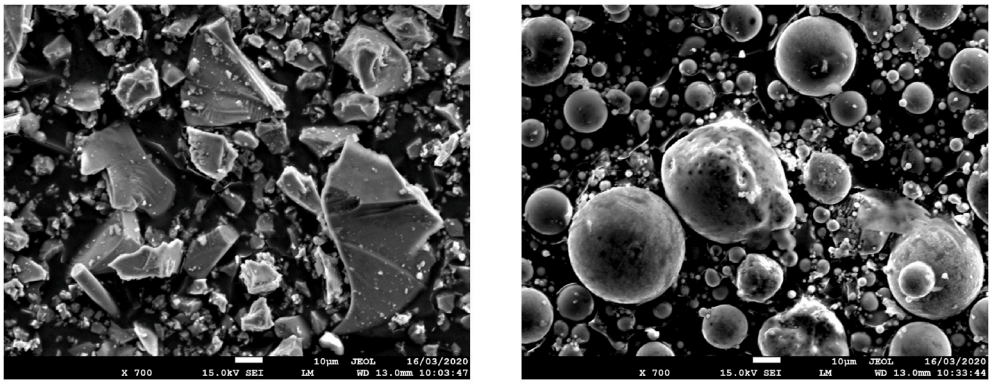

Fig. 2. SEM images of BFS and FA particles.

were then used for testing the compressive strength. The flexural strength was calculated as an average value of 3 samples, and the compressive strength was calculated as an average of 6 samples. The standard deviation was calculated as well.

3. Results and discussion

3.1. Effect of control factors on the flowability of BFS/FA-AAP

3.1.1. The Na_2O/b ratio and the SiO_2/Na_2O ratio

The effect of the Na_2O/b ratio and SiO_2/Na_2O ratio on the 5 min flowability of BFS/FA-alkali activated paste with 0.5 BFS/b and 0.4 w/b is displayed in Fig. 3. Compared with the sample activated by sodium hydroxide alone, the flowability of the sample with the introduction of sodium silicate significantly improved by 60 %–90%. Moreover, the flowability growth with SiO_2/Na_2O ratio is found to be non-linear. For example, compared with the flowability of the sample without SiO_2, the flowability of BFS/FA-AAP with SiO_2/Na_2O ratio of 0.5 increases 40–60 mm. This is probably due to the thickening of the solution [39]. The activated solution with a higher SiO_2/Na_2O ratio might provide a better coating on the surface of the precursor particles. Since the rolling friction between the particles is reduced, the flowability might keep increasing with the SiO_2/Na_2O ratio till the wrapped solution reaches a certain thickness, and the lubrication effect is fully satisfied. However, when the SiO_2/Na_2O ratio is between 0.5 and 2, the growth of flowability with the SiO_2/Na_2O ratio shows a steady and gentle trend. It is mainly because the increase in total solution volume leads to a slightly higher dispersion of the precursor particles. For example, the increase rate of the solution to water ratio with SiO_2/Na_2O ratio for BFS/FA-AAP with Na_2O/b ratio of 2%, 4%, 6%, 8%, 10% is 0.07, 0.13, 0.20, 0.27, 0.33, respectively.

Similarly, the flowability of BFS/FA-AAP increases with the increase of Na_2O/b ratio due to the higher particle dispersion. The result shows that the flowability of BFS/FA-AAP increases approximately 12 mm with every 1% increase of the Na_2O/b ratio. However, the positive effects of particle dispersion on flowability could be offset by rapid condensation. When the Na_2O/b ratio surpasses 8%, the flowability drops markedly with a higher Na_2O/b ratio. This is because a higher concentration of OH^- accelerates the dissolution process. Due to the decomposition effect of OH^-, more ions available for polymerization could be dissolved in the solution [39–41]. Besides, it is observed that this phenomenon is more obvious when SiO_2 is introduced. This is mainly because the soluble Si in the solution could further improve the condensation as a nuclear site

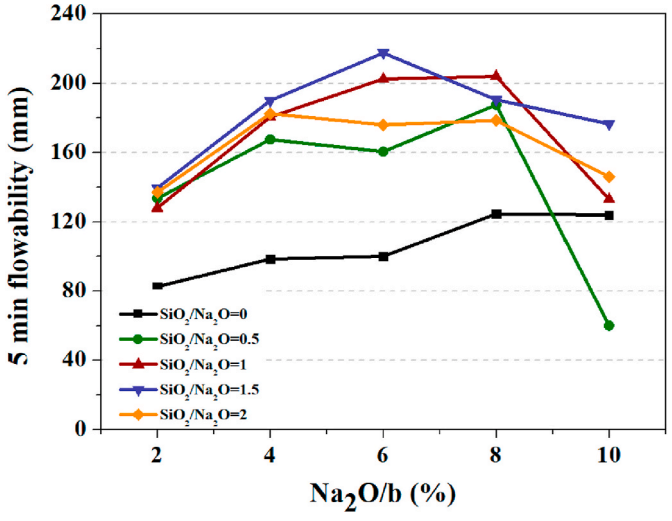

Fig. 3. Effect of Na_2O/b ratio and SiO_2/Na_2O ratio on the flowability of BFS/FA-AAP (BFS/b = 0.5; w/b = 0.4).

[42]. With every 1% increase of the Na_2O/b ratio, the flowability decreases by 0%, 34%, 17%, 4%, 9% with the SiO_2/Na_2O ratio of 0, 0.5, 1, 1.5, 2, respectively. It indicates that the reaction rate is the highest when the dissolution rate and the condensation rate reach a balance. It occurs when the SiO_2/Na_2O ratio is around 0.5–1, which shows the fastest decline in flowability.

With the progress of the reaction, the mixtures with different Na_2O/b ratios and SiO_2/Na_2O ratios show different flowability decreasing rates. As depicted in Fig. 4(a), no significant change in flowability over time is observed when the sample is activated by only sodium hydroxide. In comparison, the flowability of BFS/FA-AAP drops steadily with time when sodium silicate is introduced in the solution. It demonstrates that the reaction of BFS/FA-AAP activated by sodium silicate could be stimulated because soluble Si attracts the released reaction ions [42]. In addition, the result indicates that the flowability decreases faster with time when BFS/FA-AAP has a higher Na_2O/b ratio (see Fig. 4(b)). After 1 h, the flowability decreases by 12% and 39% when the Na_2O/b ratio is 2% and 6%, respectively. In presence of silica, the flowability of the mixtures at 15 min and after could not be tested when the Na_2O/b ratio is 10%. This could be attributed to the fast reaction rates caused by the higher concentration of OH^- and the existence of nucleation sites. As time increases, the higher the Na_2O/b ratio, the more ions could be released and absorbed by soluble Si. Hence, the flowability decreases as the polycondensation of reaction products in the systems increases.

3.1.2. The BFS/b ratio and the w/b ratio

The effect of the BFS/b ratio and the w/b ratio on the flowability of BFS/FA-AAP is presented in Fig. 5 (when Na_2O/b = 0.5; SiO_2/Na_2O = 1.5). With every 0.1 increase of the BFS/b ratio, the flowability value of BFS/FA-AAP decreases by around 6 mm. The result reveals that increasing the BFS/b ratio could reduce the flowability of BFS/FA-AAP. As shown in Fig. 2, higher content of BFS is associated with more irregular particles (BFS) and less spherical particles (FA). Accordingly, due to the increase of surface area as well as the decrease of "lubrication effect", more water is required for BFS/FA-AAP with a high BFS/b ratio to obtain appropriate workability.

Conversely, it can be seen that increasing the w/b ratio from 0.3 to 0.5 increases the flowability. This is consistent with the research of other researchers [43,44]. With every 0.1 increase in the w/b ratio, the flowability of BFS/FA-AAP increases by approximately 47 mm. In addition, when the w/b ratio is around 0.4, BFS/FA-AAP is in a plastic state (189–246 mm) in all the ranges of the BFS/b ratio. The "plastic state" refers to the state in which the paste will neither lose its flowability due to too little water nor has a bleeding problem due to too much water.

The effect of the BFS/b ratio on flowability overtime for the samples with 5% Na_2O/b, 1.5 SiO_2/Na_2O, and 0.4 w/b is shown in Fig. 6(a). The flowability of BFS/FA-AAP with a BFS/b ratio of 0 declines slowly (only 1% per hour). However, when the BFS/b ratio is 1, the flowability of BFS -AAP drops dramatically and could not be tested after 30 min. The huge difference in flowability changes is due to the different reactivity of FA and BFS at ambient temperature. Compared with BFS, FA has not only a relatively lower glassy phase content but also lower content of network modifiers (Ca) [34,35,45]. As a result, the flowability of BFS/FA-AAP with a higher BFS/b ratio tends to decrease faster over time due to a relatively higher reaction rate.

The flowability decreasing rate of BFS/FA-AAP with different w/b ratios are similar, as shown in Fig. 6(b). It suggests a weak link exists between the w/b ratio and the reaction rate. The result is consistent with previous studies which revealed that water acts merely as an alkali carrier in the alkali-activated reaction [46–49].

3.2. Effect of control factors on the setting time of BFS/FA-AAP

3.2.1. The Na_2O/b ratio and the SiO_2/Na_2O ratio

The influence of the Na_2O/b ratio and SiO_2/Na_2O ratio on the setting

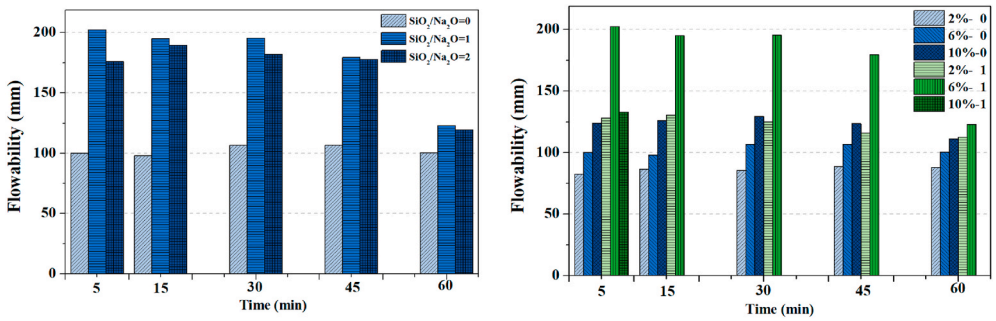

(a) BFS/b=0.5, Na_2O/b=6 %, w/b=0.4

(b) BFS/b=0.5,w/b=0.4 (legend: Na_2O/b-SiO_2/Na_2O)

Fig. 4. Effect of Na_2O/b ratio and SiO_2/Na_2O ratio on the flowability of BFS/FA-AAP with time.

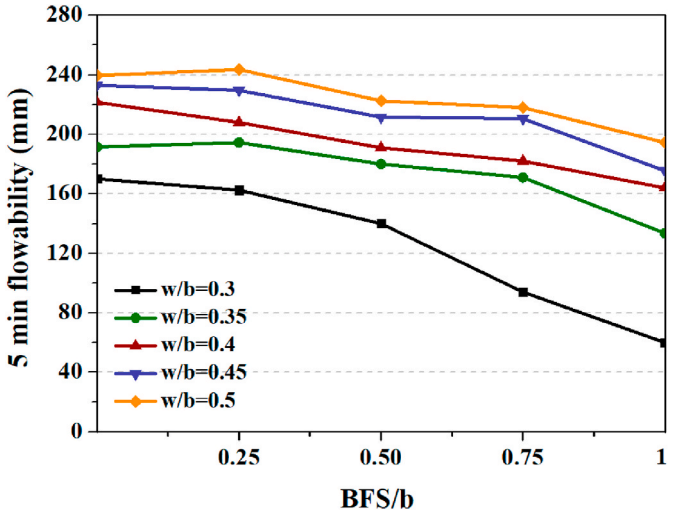

Fig. 5. Effect of BFS/b ratio and w/b ratio on flowability of BFS/FA-AAP (Na_2O/b = 0.5; SiO_2/Na_2O = 1.5).

time of mixtures with 0.5 BFS/b and 0.4 w/b is shown in Fig. 7. When the Na_2O/b ratio is 2%, BFS/FA-AAP begins to lose the plasticity at around 4 h and starts to develop strength at about 9 h. In comparison, when BFS/FA-AAP has higher alkali content (Na_2O/b ratio of 6% and 10%), the initial setting time and final setting time of BFS/FA-AAP decrease by about 56% and 74%, respectively. The result reflects that BFS/FA-AAP with a high Na_2O/b ratio tends to set faster, which is associated with a faster reaction rate. The higher concentration of OH^- can lead to an more intense attack, which releases more available reaction ions in the solution for further polymerization. The fact that increasing the Na_2O/b ratio over 6% only slightly reduced the setting time is because of the "retarding effect" of excess OH^-. When the concentration of OH^- is too high, the dissolution of $Ca(OH)_2$ is reduced, and a thin layer of $Ca(OH)_2$ might form on the surface of BFS particles [50–52]. Accordingly, the released Ca is less capable of reacting with Al and Si and forming the CASH gel. Furthermore, excess OH^- also causes Al–Si gel precipitation at the very early stage on the surface of the FA particles, so the subsequent polymerization is hindered.

In addition, it is found that BFS/FA-AAP could have a slightly lower initial setting time when SiO_2 is introduced in the system. This is consistent with the rapid flowability decrease. More soluble Si added into the reaction system could attract more released ions thus accelerating the formation speed of reaction products. On the other hand, the final setting time decreases significantly with the SiO_2/Na_2O. It is

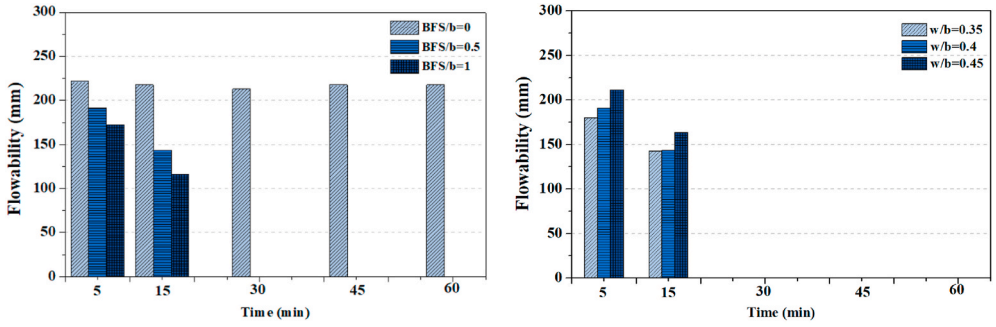

(a) Na_2O/b=5 %, SiO_2/Na_2O=1.5, w/b=0.4

(b) BFS/b=0.5, Na_2O/b=5 %, SiO_2/Na_2O=1.5

Fig. 6. Effect of BFS/b ratio and w/b ratio on the flowability of BFS/FA-AAP with time.

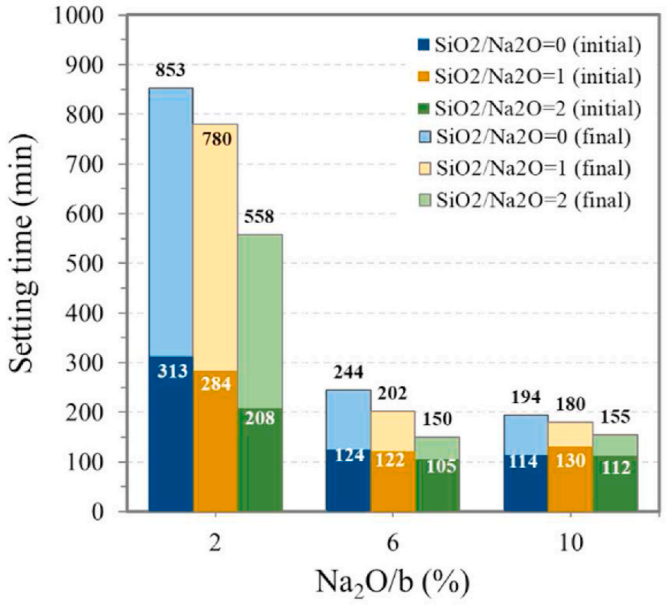

Fig. 7. Effect of the Na_2O/b ratio and the SiO_2/Na_2O ratio on setting time of BFS/FA-AAP (BFS/b = 0.5; w/b = 0.4).

reasonable because more reaction products are generated in the alkali-activated solution, thus the interparticle bonding is increased and the creation of a denser and more homogenous structure could be accelerated [53–55].

3.2.2. The BFS/b ratio and the w/b ratio

Fig. 8 illustrates the effect of the BFS/b ratio and the w/b ratio on the setting time of the mixtures with 0.5 Na_2O/b and 1.5 SiO_2/Na_2O. When the BFS/b ratio is 0, It takes around 15 h and 4 d for the paste to reach the initial setting time and final setting time, respectively. However, It is observed that the final setting time of BFS/FA-AAP can be reached within 3 h when the BFS/b ratio is 0.5, and an even shorter final setting time when BFS/b is 1.0. The big difference in setting time proves that the BFS/b ratio is the dominant control factor of setting time among the 4 control factors. Therefore, it is important to incorporate FA in BFS-AAP

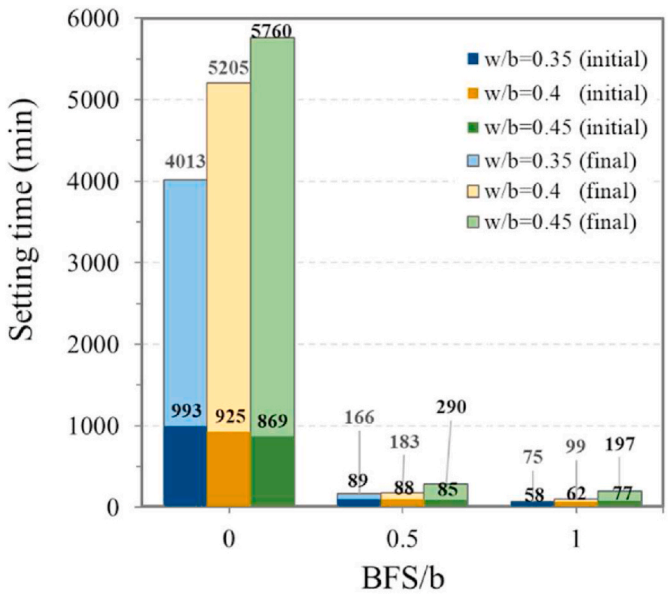

Fig. 8. Effect of BFS/b ratio and w/b ratio on setting time of BFS/FA-AAP (Na_2O/b = 0.5; SiO_2/Na_2O = 1.5).

to reach a reasonable setting time at ambient curing temperature.

It can be seen that a higher w/b ratio slightly influences the setting time of BFS/FA-AAP with low BFS content, while hardly influencing that of BFS/FA-AAP with high BFS content. When the BFS/b ratio is 0, the final setting time is increased by approximately 15 h with every 0.05 increase of the w/b ratio. On the contrary, when the BFS/b ratio of BFS/FA-AAP is 0.5–1, the increase of final setting time is around 1 h with every 0.05 increase of the w/b ratio. The influencing degree of water on the reaction of BFS/FA-AAP mainly depends on the reactivity of the precursors. If the glass phase content and network modifiers content of the precursor is high, the impact of the dilution is negligible compared with the rapid connection speed. Conversely, if the reactivity of the precursor is low, the impact of diluting alkali-activated solution could be amplified.

3.3. Effect of control factors on the strength of BFS/FA-AAP

3.3.1. The Na_2O/b ratio, the SiO_2/Na_2O ratio, and curing condition

The effect of the Na_2O/b ratio and the SiO_2/Na_2O ratio on the compressive strength of mixtures with 0.5 BFS/b, 0.4 w/b, cured under sealed condition for 90 d is presented in Fig. 9(a). Both the Na_2O/b ratio and the SiO_2/Na_2O ratios could remarkably influence compressive strength. As shown in Fig. 9(a), the compressive strength of BFS/FA-AAP first increases and then decreases with the increase of the Na_2O/b ratio. It reaches a peak when the Na_2O/b ratio is around 6 %–8%. For example, when SiO_2/Na_2O ratio is 1, the compressive strength of BFS/FA-AAPs with Na_2O/b ratio of 6% and 8% reach 80 MPa, which is twice the value of BFS/FA-AAP with a Na_2O/b ratio of 2% and 1.2 times the value of BFS/FA-AAP with a Na_2O/b ratio of 10%. It is obvious the higher content of OH^- accelerates the destruction-coagulation period [34,56,57]. The higher amount of released monomers have a higher tendency to be connected. Nevertheless, too high OH^- could lead to a negative effect on the strength because of the following reasons: 1) A $Ca(OH)_2$ layer on BFS particles hinders the formation of CASH gels. 2) The early precipitated Al–Si gel on FA particles impacts subsequent polymerization. 3) The efflorescence caused by excess Na reduces the density of the microstructure [58,59], which was observed in the specimen with 10% Na_2O in this study.

The compressive strength of BFS/FA-AAP shows an upward trend as the ratio of SiO_2/Na_2O increases in the range of 0–1. For instance, the compressive strength of BFS/FA-AAP activated by only sodium hydroxide is around 20–30 Mpa. However, when the SiO_2/Na_2O ratio rises to 1, the compressive strength of BFS/FA-AAP increases by 1.3–2.7 times. It illustrates that introducing SiO_2 in activators significantly improves the strength. The structure-forming element (Si) in the solution could act as nucleation sites, which promotes the development of strength from two aspects [57]. On the one hand, more reaction ions from the precursor particles are dissolved into the solution because the condensation on the nucleation sites keeps the undersaturation degree of reaction ions at a high level. Inevitably, the reaction is accelerated. On the other hand, since the reaction products could not only form on the surface of BFS particles but also in the solution, a denser microstructure could be generated. However, as the SiO_2/Na_2O ratio increases from 1 to 2, the increased tendency of strength is slowing down. This is because the Si in the solution keeps continuously saturated. As a result, the Si remaining on the precursor particles becomes a barrier, which hinders the further dissolution of other reaction ions [42,60]. Besides, excess SiO_2 species could precipitate in the form of polymerized SiO_4, which might inhibit the precipitation of zeolite crystals and impact the subsequent polymerization of NASH gel [61,62].

As depicted in Fig. 9(b), the effect of the Na_2O/b ratio and the SiO_2/Na_2O ratio on the flexural strength is similar to their effect on compressive strength. It is worth noting that the flexural strength value fluctuates greatly, compared with the compressive strength value. In general, the flexural strength of BFS/FA-AAP is approximately 1/9 of the compressive strength.

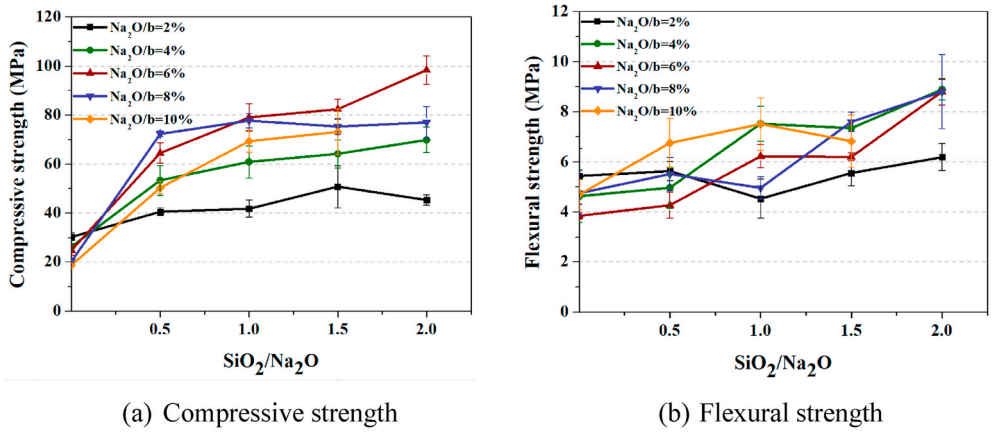

Fig. 9. Effect of Na_2O/b ratio and SiO_2/Na_2O ratio on strength of BFS/FA-AAP (BFS/b = 0.5; w/b = 0.4, cured under sealed condition for 90 d).

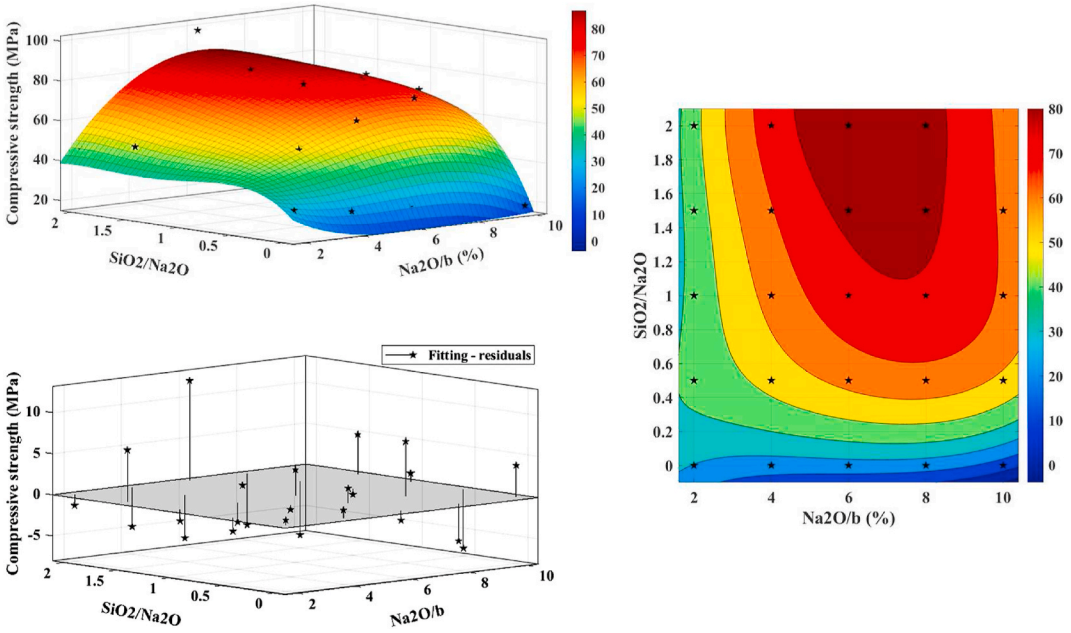

Fig. 10. Strength level of BFS/FA-AAP with different combination of the Na_2O/b ratio and the SiO_2/Na_2O (BFS/b = 0.5; w/b = 0.4, curing day = 90 d).

A polynomial fitting model is established to study the quantitative effect of the Na_2O/b ratio and the SiO_2/Na_2O ratio on the compressive strength of BFS/FA-AAP (see Fig. 10). The compressive strength is distinguished by different colors. Each degree of compressive strength (color) is related to a range of combinations of Na_2O/b ratio and SiO_2/Na_2O ratio. For example, a compressive strength higher than 80 MPa could be obtained when an appropriate combination of Na_2O/b ratio and SiO_2/Na_2O ratio is adopted (the Na_2O/b ratio = 6 %–8%; the SiO_2/Na_2O ratio = 1.2–2). An equation of polynomial surface fitting based on least squares is derived (see Eq. (1)). The R^2 of the equation is 0.88 and the confidence coefficient is 95%.

In which: X_1 is the Na_2O/b ratio (%); X_2 is the SiO_2/Na_2O ratio; $f_c(X_1, X_2, 0.4, 0.5, 90)$ is the compressive strength of BFS/FA-AAP with the w/b ratio of 0.4, the BFS/b ratio of 0.5, and sealed curing at ambient temperature for 90 days.

Despite the specimens being cured in sealed condition (sealed, 20 ± 2 °C), a batch of specimens was cured in a standard curing room (>95% relative humidity, 20 ± 2 °C) to investigate the effect of curing condition on the strength of BFS/FA-AAP. The comparison of the compressive strength of BFS/FA-AAP under two different curing conditions is shown

$$f_c(X_1,\ X_2, 0.4, 0.5, 90) = -1.33 + 12.3X_1 + 42.68X_2 - 1.04{X_1}^2 + 2.37X_1X_2 - 17.05{X_2}^2 \quad (1)$$

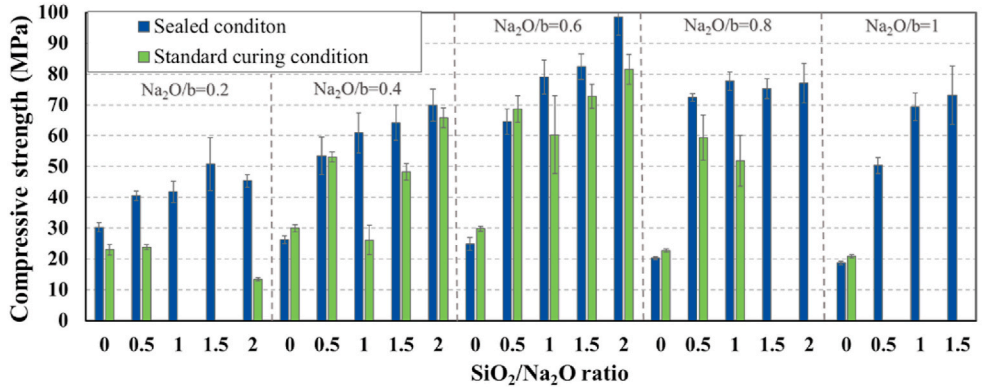

(a) Compressive strength

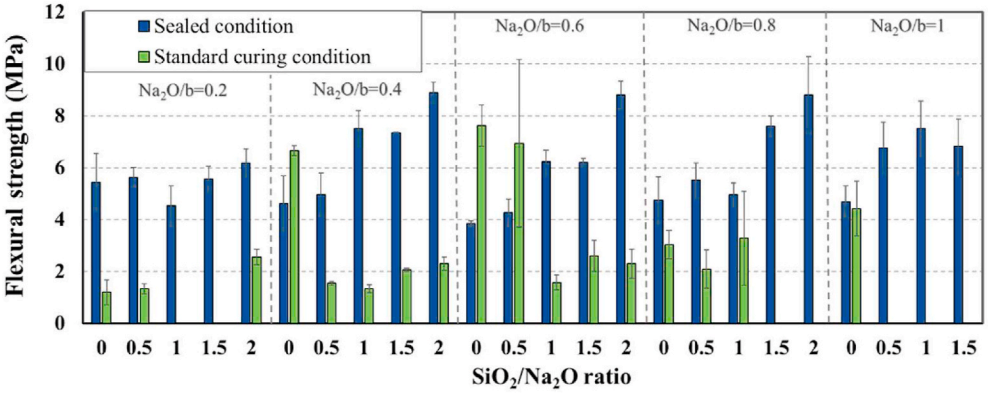

(b) Flexural strength

Fig. 11. Comparison of the strength of BFS/FA-AAP under two different curing conditions.

(a) Standard curing condition (95 % relative humidity, 20±2 ℃)

(b) Sealed condition (sealed, 20±2 ℃)

Fig. 12. Efflorescence when BFS/FA-AAP specimens are cured with high humidity.

in Fig. 11. Similar trends are found considering the effect of the Na_2O/b ratio and the SiO_2/Na_2O ratio on the compressive strength of BFS/FA-AAP. However, the compressive strength values associated with standard curing conditions fluctuate greatly and are generally 16% lower than the compressive strength associated with the sealed condition.

The fluctuating and lower compressive strength is mainly caused by the efflorescence. This is manifested in the appearance of white power ($NaHCO_3$) on the surface of specimens with a high Na_2O/b ratio. It can be observed that efflorescence occurs in BFS/FA-AAP specimens with a Na_2O/b ratio higher than 6% after 14 days of exposure in high humidity air (see Fig. 12(a)). In comparison, no efflorescence was detected in the specimens curing with sealed conditions (See Fig. 12(b)). Under a high humidity circumstance, the excess Na from the alkali activator could leach out to the pore solution and react with atmospheric CO_2 and H_2O (see Eqs. (2) and (3)) [63–65]. This shows that sealed curing could be a promising method to ensure the steady strength development of BFS/FA-AAP.

$$2NaOH + CO_2 \leftrightarrow Na_2CO_3 + H_2O \quad (2)$$

$$Na_2CO_3 + H_2O + CO_2 \leftrightarrow 2NaHCO_3 \quad (3)$$

3.3.2. The BFS/b ratio, the w/b ratio, and curing day

It is known that the strength of mortar is controlled by paste because sand has a much higher strength compared with paste [66]. For obtaining more stable compressive strength results, mortar specimens were used to study the effect of the BFS/b ratio, the w/b ratio, and curing day on the strength of BFS/FA-AAP. The mix proportion is shown

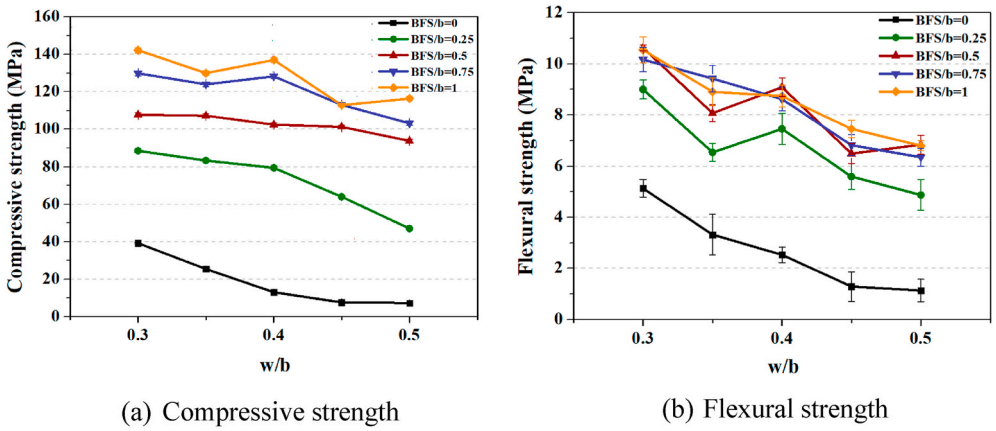

Fig. 13. Effect of BFS/b ratio and w/b ratio on strength of BFS/FA-alkali-activated mortar.

in Table 2 (experiment 2). The sand/b ratio is 3. The results are shown in Fig. 13. It is found that the strength of the sample decreases when the w/b ratio increase from 0.3 to 0.5. With every 0.1 increase of w/b ratio, the value of compressive strength and the flexural strength decrease by around 14 MPa and 2 MPa, respectively. This indicates that a denser microstructure is associated with less water content. Since water hardly participates in the alkali-activated reaction, the excess water in the materials could transform to pores, which could be harmful to strength [67–70].

In comparison, the effect of the BFS/b ratio on the strength of BFS/FA-alkali activated mortar is much larger than the effect of w/b because it greatly determines the reaction mechanism. As shown in Fig. 13(a), when the w/b ratio is 0.4 (good flowability), the compressive strength of the sample with a BFS/b ratio of 0 is 13 MPa. Compared with it, the compressive strength of the sample with a BFS/b ratio of 0.5 and 1 rise by 8 times (103 MPa) and 10 times (137 MPa), respectively. The BFS/b ratio is a key factor in compressive strength because it greatly determined the composition and structure of the reaction product. When the BFS/b ratio increases, the increase of Ca/Si and Si/Al ratios gradually results in a larger amount of CASH gel, which has a higher space-filling ability than NASH gel [18,71,72]. Due to the increasing cross-linking degree of the reaction products, a more homogenous and compacted structure is produced. Despite that, it is observed that the increase of compressive strength with the BFS/b ratio is not linear but tends to be logarithmic. With every 0.25 increase of the BFS/b ratio, the compressive strength of BFS/FA-AAP increased about 54 Mpa, 30 MPa, 17 MPa, 8 MPa, respectively. It demonstrates that the two precursors do not react separately but develop in synergy with each other to some extent [39]. The addition of a certain proportion of FA will not greatly impact the strength, but it provides the benefits of retarding setting time

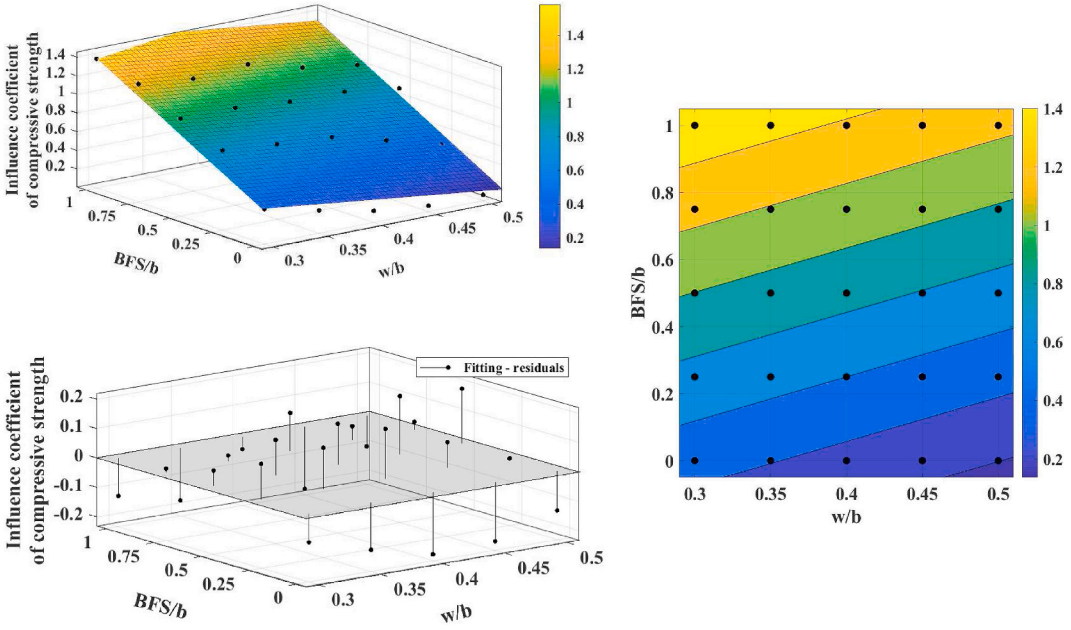

Fig. 14. Influence coefficient of compressive strength of BFS/FA-alkali activated mortar with different combinations of the BFS/b ratio and the w/b ratio (curing day = 90 d).

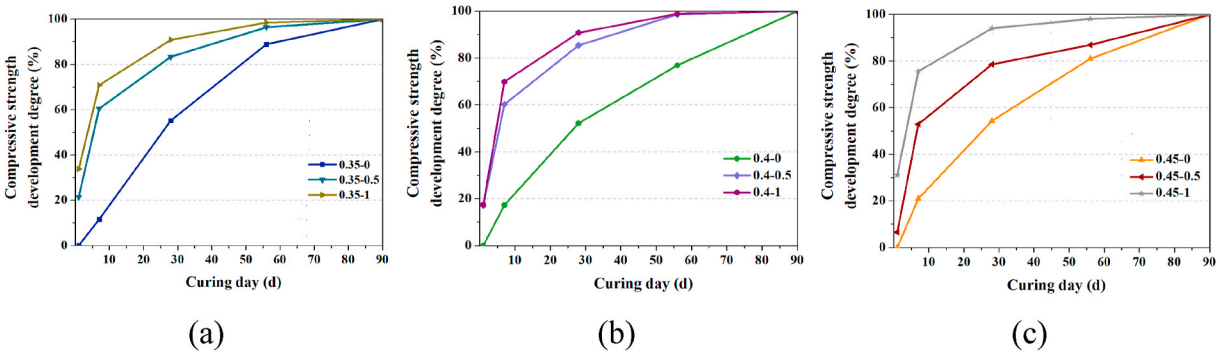

Fig. 15. The compressive strength development of BFS/FA-alkali activated mortar with different BFS/b ratios (legend: w/b-BFS/b).

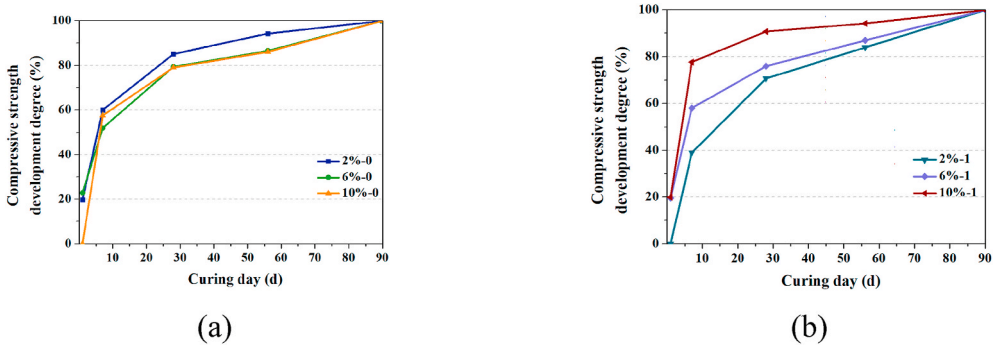

Fig. 16. The compressive strength development of BFS/FA-alkali activated mortar with different Na_2O/b ratios (legend: Na_2O/b-SiO_2/Na_2O).

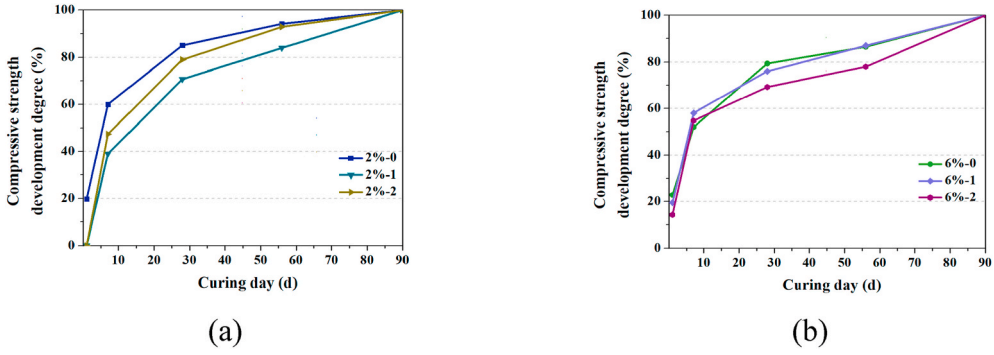

Fig. 17. The compressive strength development of BFS/FA-alkali activated mortar with different SiO_2/Na_2O ratios (legend: Na_2O/b-SiO_2/Na_2O).

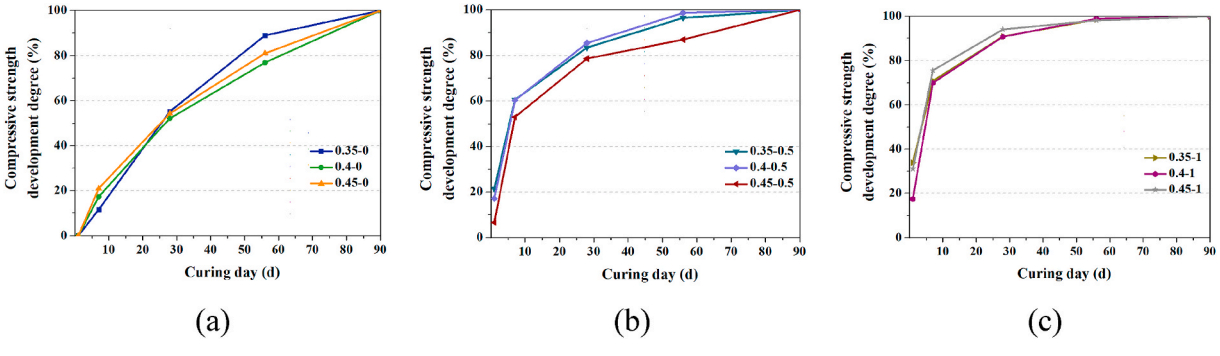

Fig. 18. The compressive strength development of BFS/FA-alkali activated mortar with different w/b ratios (legend: w/b-BFS/b).

and increasing the flowability of BFS/FA-AAM. With this consideration, a reasonably designed BFS/FA ratio of BFS/FA-AAM is crucial for the application.

Fig. 13(b) illustrates the effect of the BFS/b ratio and the w/b ratio on the flexural strength of BFS/FA-alkali-activated mortar. The effect of both factors on flexural strength is similar to their effect on compressive strength. In general, the flexural strength of BFS/FA-alkali-activated mortar is approximately 1/9 of the compressive strength.

Assuming the 90 days compressive strength of BFS/FA-alkali activated mortar with a Na_2O/b ratio of 5% and a SiO_2/Na_2O ratio of 1.5 is 1, the influence coefficient of the BFS/b ratio and the w/b ratio could be calculated, as presented in Fig. 14. The influence of the BFS/b ratio and the w/b ratio on the compressive strength could be quantitatively described by Eq. (4). The equation is derived by polynomial surface fitting based on least squares. The R^2 of the equation is 0.89 and the confidence coefficient is 95%.

$$Coe.(X_3,\ X_4) = -1.37X_3 + 1.04X_4 + 1 \quad (4)$$

In which: X_3 is the w/b ratio; X_4 is the BFS/b ratio.

Former studies have proved that the strength of BFS/FA-AAP develops till 90 days. After that, the strength of BFS/FA-AAP remains stable [12]. Assuming that the compressive strength of BFS/FA-AAP reaches 100% at 90 days, the strength development of BFS/FA-AAP with different control factors could be illustrated by Figs. 15–18.

As shown in Fig. 15, the compressive strength development degree varies a lot with different BFS/b ratios. When the BFS/b ratio is 1, the compressive strength of BFS/FA-alkali activated mortar develops logarithmically. It reaches 34%, 71%, 91%, 99%, 100% at 1 d, 7 d, 28 d, 56 d, 90 d, respectively, which indicates high early strength. However, when the BFS/b ratio is 0, the compressive strength of BFS/FA-alkali activated mortar increases nearly linearly with time. It is known that higher alkaline earth cation (Ca, Mg) gives rise to the degree of framework disorder, nonbridging oxygen atoms content as well as the formation of little content of weak and reactive Al–*O*–Al bonds [73,74]. BFS with high higher alkaline earth cation content mainly plays a role in the 28 days because the high dissolution rate accelerates the condensation of reaction products on the BFS particles, thereby hindering the further reaction. While FA with low alkaline earth cation content plays a role for a longer reaction period. It can gradually release the reaction ions and continually contribute to the strength till 90 days. As a result, the higher the BFS/b ratio, the earlier the compressive strength develops. It should be pointed out that the compressive strength development speed of the sample with a BFS/b ratio of 0.5 is only slightly lower than that of the sample with a BFS/b ratio of 1. It reaches 17%, 60%, 85%, 99%, 100% at 1 d, 7 d, 28 d, 56 d, 90 d, respectively. This further illustrates that the FA can promote the BFS reaction by acting as a coagulation nucleus [42]. More NASH gel is formed later and gradually fills the pores. Furthermore, because of the exchange of Al and Ca in the restructuration of CASH gel and NASH gel, a homogeneous structure is produced [39,75].

The strength development of BFS/FA-alkali activated mortar with different Na_2O/b ratios is presented in Fig. 16. When BFS/FA-alkali activated mortar is activated by only sodium hydroxide, the compressive strength development is similar regardless of the alkali concentration. However, when SiO_2 is introduced, the sample with a higher Na_2O/b ratio tends to have higher early strength. This is because the soluble Si in the solution could keep the saturation degree of reaction ions (except Si) at a low level. In the meantime, an activator with higher OH^- is more capable of dissolving precursor particles.

The effects of different SiO_2/Na_2O ratios and w/b ratios on the strength development of BFS/FA-alkali activated mortar is shown in Figs. 17 and 18, respectively. The results show that the effect of SiO_2/Na_2O ratio and w/b ratio on compressive strength development of BFS/FA-AAP is negligible.

Assuming the 90 days compressive strength of BFS/FA-alkali activated mortar is 1, an equation based on least squares is derived to evaluate the compressive strength degree of BFS/FA-alkali activated mortar at different ages (see Eq. (5)). The R^2 of the equation is 0.71 and the confidence coefficient is 95%.

$$Coe.(X_5) = 0.2\ln(X_5 + 11.31) \quad (5)$$

In which: X_5 is the curing day.

3.4. A mix design method of BFS/FA-AAP

3.4.1. Evaluation of early age properties

Based on the fitting results above, a strength predictive formula could be obtained considering 5 control factors, including Na_2O/b ratio, SiO_2/Na_2O ratio, w/b ratio, BFS/b ratio, and curing days (see Eq. (6)). The formula is derived by multiplying Eq. (1) with the adjustment coefficient Eqs. (4) and (5). It could be used to evaluate the compressive strength of BFA/FA-AAP when the Na_2O/b ratio is between 0 % and 10%, the SiO_2/Na_2O ratio is between 0 and 2, the w/b ratio is between 0.3 and 0.5, the BFS/b ratio is between 0 and 1, and sealed curing at ambient temperature.

$$f_c(X_1, X_2,\ X_3,\ X_4,\ X_5) = \left(-1.33 + 12.3X_1 + 42.68X_2 - 1.04{X_1}^2 + 2.37X_1X_2 - 17.05{X_2}^2\right)\cdot(-1.37X_3 + 1.04X_4 + 1)\cdot 0.2\ln(X_5 + 11.31) \quad (6)$$

In which: X_1 is the Na_2O/b ratio (%); X_2 is the SiO_2/Na_2O ratio; X_3 is the w/b ratio; X_4 is the BFS/b ratio; X_5 is the curing days (d); $f_c(X_1, X_2, X_3, X_4, X_5)$ is the compressive strength of BFS/FA-AAP that is sealed and cured at ambient temperature (MPa).

To verify the strength predictive formula, 100 data points from 5 pieces of literature related to the compressive strength of BFS/FA-AAM have been collected. All data in the literature are from mortar samples cured under unsealed conditions. According to the mixed proportion and the characteristic of the raw materials of each sample, the relative control factors were first calculated. Afterward, the predictive compressive strength of each sample was calculated by Eq. (6). The final predicted results were obtained by multiplying the predicted value by an unsealed curing reduction coefficient of 0.84 (the coefficient value could be obtained from the results in section 3.3.1). Eventually, the final predictive compressive strength results were compared with the real experimental results (see Fig. 19).

The Pearson correlation coefficient of predictive value and test value is 0.88, indicating that there is a high degree of linear positive correlation between them. The error values could be obtained by subtracting the test value from the predicted value. It is found that 59% of data points have an error value within 10 MPa, and 90% of data points have an error value within 15 MPa. A Wilcoxon signed-rank test is conducted by SPSS to statistically evaluate the validity of predictive data. According to the test results, the median of the test value is 46 MPa, the median of the predictive value is 47 MPa, and the median of error is −1.34 MPa. The P-value of test value and predictive value is 0.75, which indicates that the difference between the two groups is statistically insignificant. The deviations mainly come from strength fluctuation caused by unsealed curing (as illustrated in Fig. 11). In conclusion, Eq. (6) could generally evaluate the compressive strength of BFS/FA-AAP. However, to achieve high repeatability, further research should be

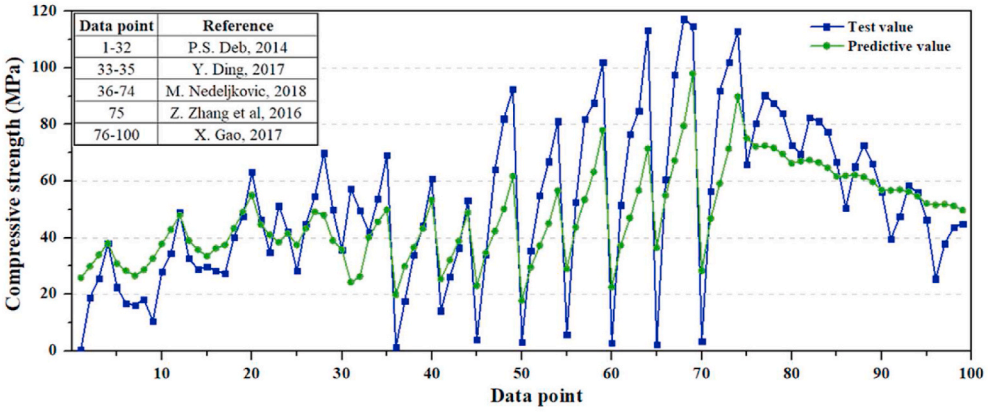

Fig. 19. Verification of the compressive strength predictive formula.

conducted to reduce errors caused by the following possible reasons: 1) the different chemical composition and particle size of precursors; 2) the different curing conditions; 3) the different operations.

The predictive flexural strength of BFS/FA-AAP could be obtained by dividing the predicted result of compressive strength by 9. Moreover, the 5 min flowability of BFS/FA-AAP and the setting time could be evaluated by linear interpolation of the test results in sections 3.1 and 3.2. Accordingly, the 3 most important properties of BFS/FA-AAP could be calculated. And a mix design method could be proposed based on the principle of satisfying the requirement of strength, flowability, and setting time.

3.4.2. A mix design method of BFS/FA-AAP

In order to carry out a simple approach for mix design of BFS/FA-AAP, the BFS/FA-AAP design table is proposed (see Table 3). This table could be used to do the mix design of BFS/FA-AAP considering early properties (durability is not included). The AAP grade is the same as the cement grade, which represents the compressive strength. For example, 42.5 means that the compressive strength of BFS/FA-AAP after hardening for 90 days (relatively stable strength) is 42.5 MPa. Besides, a series of symbols are used to represent the different range of flowability values. Light symbols mean high flowability, while dark symbols mean low flowability. As a reference, the 5 min flowability of cement paste

Table 3
BFS/FA-AAP design table.

Mix design of AAP	AAP grade	BFS/b	Na_2O/b (%)				
			2	4	6	8	10
			SiO_2/Na_2O				
w/b=0.4	32.5 (C30)	0			0.89-2.45 ☆	0.90-2.71 □◇☆	1.18-2.71 ◈○△□
Note: with every 0.1 increase of w/b ratio, compressive strength decreases by 14 Mpa, flowability increases by 47 mm		0.25	0.78-2 ◭◧	0.31-0.72 ◧◈○	0.20-0.52 ◉◭◧◈	0.27-0.56 ○△□	0.48-0.80 ●▲■◆
		0.5	0.35-0.69 ■◆★◉	0.04-0.26 ■◆★	0-0.16 ◆	0.05-0.23 ★◉◭	0.26-0.44 ●▲■
		0.75	0.16-0.38 ▲■◆	0-0.07 ■		0-0.07 ★	0.14-0.27 ▲■
		1	0.06-0.22 ●▲				0.06-0.17 ■
Setting time (min)	42.5 (C40)	0.25		0.72-2.34 △□	0.52-0.96 ○△□◇	0.56-0.96 □◇	0.80-1.25 ★◉◭◧◈
Initial>45 Final<600		0.5	0.69-2.09 ◉	0.26-0.53 ◉◭◧	0.16-0.38 ◆★◉	0.23-0.44 ◧◈	0.44-0.66 ●▲
Initial>240 Final>600		0.75	0.38-0.65 ◆★	0.07-0.24 ■◆★	0-0.14 ■	0.07-0.21 ◉	0.27-0.42 ●▲
		1	0.22-0.40 ▲■	0-0.08 ▲		0-0.08 ◆	0.17-0.29 ▲
5 min flowability	52.5 (C50)	0.25			0.96-2 △□◇	0.96-3 △□◇	1.25-2.65 ◈○△
Note: flowability increases with SiO_2/Na_2O ratio		0.5		0.53-0.90 ◈	0.38-0.64 ◭◧◈	0.44-0.68 ○△	0.66-0.92 ■◆★◉
		0.75	0.65-1.12 ★	0.24-0.44 ★◉◭	0.14-0.31 ◆★	0.21-0.37 ◭◧	0.42-0.59 ●
● 80-90 mm		1	0.40-0.62 ◆	0.08-0.22 ▲■	0-0.13 ▲	0.08-0.20 ◆★	0.29-0.41 ●
▲ 90-100 mm	62.5 (C60)	0.5		0.90-2.16 ○	0.64-0.99 ◈	0.68-0.99 △	0.92-1.28 ◉◭◧
■ 100-110 mm		0.75	1.12-1.66 ★◉	0.44-0.68 ◧	0.31-0.49 ◉◭	0.37-0.54 ◧◈○	0.59-0.78 ●▲
◆ 110-120 mm		1	0.62-0.94 ◆	0.22-0.38 ◆★	0.13-0.26 ■	0.20-0.32 ◉	0.41-0.54 ●
★ 120-130 mm	72.5 (C70)	0.5			0.99-2.34 ○	0.99-1.55 △	1.28-2.61 ◧◈
◉ 130-140 mm		0.75		0.68-1.04 ◈	0.49-0.72 ◧◈	0.54-0.75 ○	0.78-1 ■◆★
◭ 140-150 mm		1	0.94-1.84 ◆★	0.38-0.57 ★◉	0.26-0.41 ◆★	0.32-0.46 ◭	0.54-0.69 ●
◧ 150-160 mm	82.5 (C80)	0.5				1.55-2.07 ○	
◈ 160-170 mm		0.75		1.04-2.02 ◈○	0.72-1.01 ◈○△	0.75-1 ○△	1-1.30 ◉◭
○ 170-180 mm		1		0.57-0.80 ◭	0.41-0.57 ◉	0.46-0.62 ◧	0.69-0.86 ▲■
△ 180-190 mm	92.5 (C90)	0.75			1.01-2.32 △□	1-1.40 △□	1.30-2.59 ◭◧◈
□ 190-200 mm		1		0.80-1.16 ◭◧	0.57-0.77 ◭	0.62-0.80 ◈	0.86-1.06 ◆
◇ 200-210 mm	>102.5 (C100)	0.75				1.40-2.22 ○△□	
☆ 210-240 mm		1		1.16-1.90 ◧	0.77-2.57 ◧◈	0.80-2.82 ◈	1.06-2.84 ★◉◭

with cement grade 52.5 and w/b ratio of 0.5 is 118 mm. According to the setting time, BFS/FA-AAP could be classified into 2 categories. The green part in the table represents BFS/FA-AAP with the initial setting time higher than 45 min and the final setting time lower than 600 min, which is the same as the setting time of normal cement. While the blue part is associated with the BFS/FA-AAP with an initial setting time higher than 240 min and a final setting time higher than 600 min. It is worth noting that the w/b ratio in Table 3 is 0.4. Based on that, with every 0.01 increase of w/b ratio, the compressive strength is expected to decrease by around 1.4 MPa, the flowability is expected to increase by approximately 4.7 mm, the initial setting time and final setting time are expected to decrease by 1.4% and 4.5%, respectively.

The selection of a mix proportion depends on the requirements for early performance, as well as the availability and the price of raw materials. For example, a BFS/FA-AAP with compressive strength of 42.5 MPa, the flowability of 145 mm, initial setting time higher than 45 min, and final setting time lower than 600 min could be designed by the following process:

1) According to the requirements of the compressive strength and the setting time, all mix proportions in the green parts of the AAP 42.5 interval could be pre-selected as potential mixes.
2) According to the requirement of flowability, all mixes with a symbol: ◭ could be further selected. Considering no mix in the pre-selected area meets this requirement. The w/b ratio should be adjusted based on the suggestion on the left side of the table.
3) Before adjusting the w/b ratio, a mix proportion should be selected in the preselected range based on the principle of enlarging the content of easily available, cheap, and environmentally friendly raw materials. Considering the higher availability of BFS and the economic benefit of using an activator with a lower alkali concentration, the mix proportion to be adjusted should be: BFS/b ratio of 0.75, Na_2O/b ratio of 4%, SiO_2/Na_2O ratio of 0.24. It has suitable strength and setting time but a lower flowability (125 mm).
4) For increasing the flowability of the selected mix by 20 mm, the w/b ratio should increase to 0.44. For compensating the compressive strength loss (around 6 MPa), the following measurements could be taken: a) increase the BFS/b ratio (with every 0.1 increase of the BFS/b ratio, the compressive strength increases by 10 MPa, the flowability decreases by 6 mm); b) increase the Na_2O/b ratio (when the Na_2O/b ratio is lower than 6%, with every 1% increase of it, the compressive strength increases by 9 MPa, the flowability increases by 12 mm); c) increase the SiO_2/Na_2O ratio (when the SiO_2/Na_2O ratio is lower than 0.5, with every 0.1 increase of it, the compressive strength increases by 6 Mpa, the flowability increases by 12 mm). Therefore, the final mix proportion could be: BFS/b ratio of 0.75, Na_2O/b ratio of 4%, SiO_2/Na_2O ratio of 0.34, w/b ratio of 0.42.

4. Conclusions

This paper investigated the effect of control factors on the early age properties of BFS/FA-AAP, i.e., strength development, flowability development, and setting time. The predictive methods of these properties are derived by fitting the experimental data. A mix design table is proposed for designing BFS/FA-AAP. According to the results, the main conclusions could be extracted as follow:

(1) At the early stage, a higher SiO_2/Na_2O ratio, lower BFS/b ratio, and higher w/b ratio could lead to higher workability. Within the normal design range, the influence ranking is: BFS/b ratio $\geq$ w/b ratio $>$ SiO_2/Na_2O ratio. As time goes by, the workability of BFS/FA-AAP with a higher Na_2O/b ratio and BFS/b ratio decreases dramatically due to the high reaction rate.
(2) The setting time of BFS/FA-AAP increases with the increase of w/b ratio and increases with the decrease of Na_2O/b ratio, BFS/b ratio, and SiO_2/Na_2O ratio. Within the normal design range, the order of the influence is: BFS/b ratio $>$ Na_2O/b ratio $>$ SiO_2/Na_2O ratio $>$ w/b ratio.
(3) The compressive strength of BFS/FA-AAP increases with the increase of BFS/b ratio, the decrease of w/b ratio, and the appropriate combination of the Na_2O/b ratio and the SiO_2/Na_2O ratio. Generally, the BFS/FA-AAP with a Na_2O/b ratio of 6 %–8% and a SiO_2/Na_2O ratio of around 1–2 could reach the highest compressive strength. Among all factors, the BFS/b ratio contributes the most to the compressive strength, while the w/b ratio has the least influence on compressive strength. Compared with normal curing, sealed curing could enhance the compressive strength of BFS/FA-AAP by about 35%.
(4) The flexural strength of BFS/FA-AAP has relatively larger fluctuation than the compressive strength of BFS/FA-AAP. Besides, the flexural strength of BFA/FA AAP is generally 1/9 of the compressive strength.
(5) The predictive compressive strength formula of BFS/FA-AAP derived in this research is proved to be effective by verification. The flowability and setting time could be calculated as well. Accordingly, the 3 early age properties of any BFS/FA-AAP within the range of this study could be evaluated.
(6) Considering the satisfaction of the 3 early properties, The BFS/FA-AAP could be preliminary designed according to the mix design table, which included most of the mix proportion combinations. Afterward, the adjustment could be made by understanding how different control factors influence workability and strength, which have been clarified in this paper.
(7) In future research, A BFS/FA-based alkali-activated concrete mix design method is expected to be built since the conventional concrete code is not applicable. Besides, more secondary influencing factors (such as the chemical composition and particle size of precursors, the curing temperature, etc.) need to be studied to modify the predictive method.

Declaration of competing interest

The authors declare that they have no known competing financial interests or personal relationships that could have appeared to influence the work reported in this paper.

Acknowledgments

The first author also would like to gratefully acknowledge the China Scholarship Council (Grant Number 201806370216).

Appendix A. Supplementary data

Supplementary data to this article can be found online at https://doi.org/10.1016/j.cemconcomp.2021.104368.

References

[1] G. Habert, J.D.E. De Lacaillerie, N. Roussel, An environmental evaluation of geopolymer based concrete production: reviewing current research trends, J. Clean. Prod. 19 (11) (2011) 1229–1238.
[2] L.K. Turner, F.G. Collins, Carbon dioxide equivalent (CO2-e) emissions: a comparison between geopolymer and OPC cement concrete, Construct. Build. Mater. 43 (2013) 125–130.
[3] J.S. van Deventer, J.L. Provis, P. Duxson, D.G. Brice, B. Valorization, Chemical research and climate change as drivers in the commercial adoption of alkali activated materials, Waste and Biomass Valorization 1 (1) (2010) 145–155.
[4] J. Davidovits, Geopolymer cements to minimize carbon dioxide greenhouse warming, Ceram. Trans. 37 (1) (1993) 165–182.
[5] N. Marjanović, M. Komljenović, Z. Baščarević, V. Nikolić, Comparison of two alkali-activated systems: mechanically activated fly ash and fly ash-blast furnace slag blends, Procedia Eng. 108 (2015) 231–238.
[6] M.A. Yazdi, M. Liebscher, S. Hempel, J. Yang, V. Mechtcherine, Correlation of microstructural and mechanical properties of geopolymers produced from fly ash and slag at room temperature, Construct. Build. Mater. 191 (2018) 330–341.

[7] A. Wardhono, D.W. Law, Sutikno, H. Dani, The effect of slag addition on strength development of Class C fly ash geopolymer concrete at normal temperature, AIP Conf. Proc. 1887 (2017) 1–7.
[8] A. Kothari, Effects of Fly Ash on the Properties of Alkali Activated Slag Concrete, 2017.
[9] P.S. Deb, P. Nath, P.K. Sarker, The effects of ground granulated blast-furnace slag blending with fly ash and activator content on the workability and strength properties of geopolymer concrete cured at ambient temperature, Mater. Des. 62 (2014) 32–39, 1980-2015.
[10] A. Mehta, R. Siddique, T. Ozbakkaloglu, F. Uddin Ahmed Shaikh, R. Belarbi, Fly ash and ground granulated blast furnace slag-based alkali-activated concrete: mechanical, transport and microstructural properties, Construct. Build. Mater. 257 (2020).
[11] W.C. Wang, H.Y. Wang, M.H. Lo, The fresh and engineering properties of alkali activated slag as a function of fly ash replacement and alkali concentration, Construct. Build. Mater. 84 (2015) 224–229.
[12] M. Nedeljkovic, Z. Li, G. Ye, Setting, strength, and autogenous shrinkage of alkali-activated fly ash and slag pastes: effect of slag content, Materials 11 (11) (2018).
[13] S.Y. Oderji, B. Chen, M.R. Ahmad, S.F.A. Shah, Fresh and hardened properties of one-part fly ash-based geopolymer binders cured at room temperature: effect of slag and alkali activators, J. Clean. Prod. 225 (2019) 1–10.
[14] G. Vikas, T.D. Rao, Setting time, workability and strength properties of alkali activated fly ash and slag based geopolymer concrete activated with high silica modulus water glass, Iran. J. Sci. Technol. Trans. Civ. Eng. (2021) 1–10.
[15] G. Fang, W.K. Ho, W. Tu, M. Zhang, Workability and mechanical properties of alkali-activated fly ash-slag concrete cured at ambient temperature, Construct. Build. Mater. 172 (2018) 476–487.
[16] A.M. Humad, A. Kothari, J.L. Provis, A. Cwirzen, The effect of blast furnace slag/fly ash ratio on setting, strength, and shrinkage of alkali-activated pastes and concretes, Front. Mater. 6 (2019).
[17] S. Samantasinghar, S.P. Singh, Fresh and hardened properties of fly ash–slag blended geopolymer paste and mortar, Int. J. Concr. Struct. Mater. 13 (1) (2019) 1–12.
[18] X. Ouyang, Y. Ma, Z. Liu, J. Liang, G. Ye, Effect of the sodium silicate modulus and slag content on fresh and hardened properties of alkali-activated fly ash/slag, Materials 10 (1) (2020) 15.
[19] S. Saha, C. Rajasekaran, Enhancement of the properties of fly ash based geopolymer paste by incorporating ground granulated blast furnace slag, Construct. Build. Mater. 146 (2017) 615–620.
[20] B. Singh, M.R. Rahman, R. Paswan, S.K. Bhattacharyya, Effect of activator concentration on the strength, ITZ and drying shrinkage of fly ash/slag geopolymer concrete, Construct. Build. Mater. 118 (2016) 171–179.
[21] A.M. Rashad, Engineering, Properties of alkali-activated fly ash concrete blended with slag, Irian J. Mater. Sci. Eng. 10 (1) (2013) 57–64.
[22] M. Chi, R. Huang, Binding mechanism and properties of alkali-activated fly ash/slag mortars, Construct. Build. Mater. 40 (2013) 291–298.
[23] P. Nath, P.K. Sarker, Flexural strength and elastic modulus of ambient-cured blended low-calcium fly ash geopolymer concrete, Construct. Build. Mater. 130 (2017) 22–31.
[24] R. Anuradha, V. Sreevidya, R. Venkatasubramani, B.V. Rangan, Modified guidelines for geopolymer concrete mix design using Indian standard, Asian J. Civ. Eng. (2012) 13.
[25] M.S. Reddy, P. Dinakar, B.H. Rao, Mix design development of fly ash and ground granulated blast furnace slag based geopolymer concrete, J. Build. Eng. 20 (2018) 712–722.
[26] A. Rafeet, R. Vinai, M. Soutsos, W. Sha, Guidelines for mix proportioning of fly ash/GGBS based alkali activated concretes, Construct. Build. Mater. 147 (2017) 130–142.
[27] M.T. Junaid, O. Kayali, A. Khennane, J. Black, A mix design procedure for low calcium alkali activated fly ash-based concretes, Construct. Build. Mater. 79 (2015) 301–310.
[28] M.N. Hadi, N.A. Farhan, M.N.J.C. Sheikh, Design of geopolymer concrete with GGBFS at ambient curing condition using Taguchi method, B. Construct. Build. Mater. 140 (2017) 424–431.
[29] R.R. Bellum, R. Nerella, S.R.C. Madduru, C.S.R. Indukuri, Mix design and mechanical properties of fly ash and GGBFS-synthesized alkali-activated concrete (AAC), Infrastructure 4 (2) (2019) 20.
[30] M.N. Hadi, H. Zhang, S. Parkinson, Optimum mix design of geopolymer pastes and concretes cured in ambient condition based on compressive strength, setting time and workability, J. Build. Eng. (2019) 301–313.
[31] N. Li, C. Shi, Z. Zhang, H. Wang, Y. Liu, A review on mixture design methods for geopolymer concrete, Compos. B Eng. 178 (2019) 107490.
[32] F. Collins, J.G. Sanjayan, Workability and mechanical properties of alkali activated slag concrete, Cement Concr. Res. 29 (3) (1999) 455–458.
[33] J. Xie, J. Wang, R. Rao, C. Wang, C. Fang, Effects of combined usage of GGBS and fly ash on workability and mechanical properties of alkali activated geopolymer concrete with recycled aggregate, Compos. B Eng. 164 (2019) 179–190.
[34] S.D. Wang, K.L. Scrivener, P.L. Pratt, Factors affecting the strength of alkali-activated slag, Cement Concr. Res. 24 (6) (1994) 1033–1043.
[35] B. Talling, J. Brandstetr, Present state and future of alkali-activated slag concretes, 114, 1989, pp. 1519–1546.
[36] W. Bumrongjaroen, I. Muller, R. Livingston, J. Schweitzer, Fly Ash Reactivity as a Glass Corrosion Topic, 12th International Congress on the Chemistry of Cement, Kanada, Montreal, 2007.
[37] E.I.D. Loya, F. Kinney, C. Rios, Reactivity indicators for activated high-calcium fly ash-based binders, Adv. Green Binder Sys. 294 (2013) 1–22.
[38] R. Siddique, M.I. Khan, Supplementary Cementing Materials, Springer Science & Business Media, 2011.
[39] C. Shi, D. Roy, P. Krivenko, Alkali-activated Cements and Concretes, CRC press, 2003.
[40] V. Glukhovsky, Ancient, modern and future concretes, in: Proceedings of the First International Conference on Alkaline Cements and Concretes, Kiev, Ukraine, 1994, pp. 1–9.
[41] A. Palomo, P. Krivenko, I. Garcia-Lodeiro, E. Kavalerova, O. Maltseva, A. Fernández-Jiménez, A review on alkaline activation: new analytical perspectives, Mater. Construcción 64 (315) (2014).
[42] Y. Zuo, Experimental Study and Numerical Simulation of the Reaction Process and Microstructure Formation of Alkali-Activated Materials, Delft University of Technology, 2019.
[43] J. Zhang, Y. Ma, J. Zheng, J. Hu, J. Fu, Z. Zhang, H. Wang, Chloride diffusion in alkali-activated fly ash/slag concretes: role of slag content, water/binder ratio, alkali content and sand-aggregate ratio, Construct. Build. Mater. 261 (2020) 119940.
[44] M. Al-Majidi, A. Lampropoulos, A. Cundy, Effect of alkaline activator, water, superplasticiser and slag contents on the compressive strength and workability of slag-fly ash based geopolymer mortar cured under ambient temperature, Int. J. Civ. Environ. Construct. Architect. Eng. 4 (2016) 6.
[45] W.H. Zachariasen, The atomic arrangement in glass, J. Am. Chem. Soc. 54 (10) (1932) 3841–3851.
[46] F. Skvara, L. Kopecky, V. Smilauer, Z. Bittnar, Material and structural characterization of alkali activated low-calcium brown coal fly ash, J. Hazard Mater. 168 (2–3) (2009) 711–720.
[47] H. Xu, J.S.J. van Deventer, The effect of alkali metals on the formation of geopolymeric gels from alkali-feldspars, S.A. Physicochem. E. Aspects 216 (1–3) (2003) 27–44.
[48] J. Davidovits, Geopolymer Chemistry and Properties, Geopolymer, 1988, pp. 25–48.
[49] D. Hardjito, B.V. Rangan, Development and Properties of Low-Calcium Fly Ash-Based Geopolymer Concrete, 2005.
[50] J. Li, Q. Yu, H. Huang, S. Yin, Difference in the reaction process of slag activated by waterglass solution and NaOH solution, Struct. Concr. 20 (5) (2019) 1528–1540.
[51] C. Yip, J.S.J. van Deventer, Microanalysis of calcium silicate hydrate gel formed within a geopolymeric binder, J. Mater. Sci. 38 (18) (2003) 3851–3860.
[52] N. Marjanović, M. Komljenović, Z. Baščarević, V. Nikolić, R. Petrović, Physical–mechanical and microstructural properties of alkali-activated fly ash–blast furnace slag blends, Ceram. Int. 41 (1) (2015) 1421–1435.
[53] I.G. Richardson, A.R. Brough, G.W. Groves, C.M. Dobson, The characterization of hardened alkali-activated blast-furnace slag pastes and the nature of the calcium silicate hydrate (CSH) phase, Cement Concr. Res. 24 (5) (1994) 813–829.
[54] I. Lecomte, C. Henrist, M. Liégeois, F. Maseri, A. Rulmont, R. Cloots, (Micro)-structural comparison between geopolymers, alkali-activated slag cement and Portland cement, J. Eur. Ceram. Soc. 26 (16) (2006) 3789–3797.
[55] V. Živica, Effects of type and dosage of alkaline activator and temperature on the properties of alkali-activated slag mixtures, Construct. Build. Mater. 21 (7) (2007) 1463–1469.
[56] F. Puertas, S. Martínez-Ramírez, S. Alonso, T.J.C. Vazquez, Alkali-activated fly ash/slag cements: strength behaviour and hydration products, Cement Concr. Res. 30 (10) (2000) 1625–1632.
[57] Z. Shi, C. Shi, S. Wan, Z. Zhang, Effects of alkali dosage and silicate modulus on alkali-silica reaction in alkali-activated slag mortars, Cement Concr. Res. 111 (2018) 104–115.
[58] F. Škvára, V. Šmilauer, P. Hlaváček, L. Kopecký, Z. Cilova, A weak alkali bond in (N, K)–A–S–H gels: evidence from leaching and modeling, 56, 2012, pp. 374–382, 4.
[59] A. Allahverdi, E.N. Kani, S. Esmaeilpoor, Effects of silica modulus and alkali concentration on activation of blast-furnace slag, Iran. J. Mater. Sci. Eng. 5 (2) (2008) 32–35.
[60] A.S. De Vargas, D.C.C. Dal Molin, A.C.F. Vilela, F.J.D. Silva, B. Pavão, H. Veit, The effects of Na2O/SiO2molar ratio, curing temperature and age on compressive strength, morphology and microstructure of alkali-activated fly ash-based geopolymers, Cement Concr. Compos. 33 (6) (2011) 653–660.
[61] V. Labet, P. Colomban, Vibrational properties of silicates: a cluster model able to reproduce the effect of "SiO4" polymerization on Raman intensities, J. Non-Cryst. Solids 370 (2013) 10–17.
[62] K. Okada, Y. Kameshima, A. Yasumori, Chemical shifts of silicon X-ray photoelectron spectra by polymerization structures of silicates, J. Am. Ceram. Soc. 81 (7) (1998) 1970–1972.
[63] E.N. Kani, A. Allahverdi, J.L. Provis, Efflorescence control in geopolymer binders based on natural pozzolan, Cement Concr. Compos. 34 (1) (2012) 25–33.
[64] F. Škvára, L. Kopecký, L. Myšková, V. Šmilauer, L. Alberovska, L. Vinšová, Aluminosilicate polymers–influence of elevated temperatures, efflorescence, Ceram. Int. 53 (4) (2009) 276–282.
[65] A. Saludung, T. Azeyanagi, Y. Ogawa, K. Kawai, Effect of silica fume on efflorescence formation and alkali leaching of alkali-activated slag, J. Clean. Prod. 315 (2021) 128210.
[66] P.K. Mehta, P.J. Monteiro, Concrete: Microstructure, Properties, and Materials, McGraw-Hill Education, 2014.
[67] S.A. Bernal, J.L. Provis, J.S. van Deventer, Impact of water content on the performance of alkali-activated slag concretes, Int. Conf. Durab. Concr. Struct. (2019).
[68] J. Shekhovtsova, E.P. Kearsley, M. Kovtun, Effect of activator dosage, water-to-binder-solids ratio, temperature and duration of elevated temperature curing on

the compressive strength of alkali-activated fly ash cement pastes, J. S. Afr. Inst. Civ. Eng. 56 (3) (2014) 44–52.
[69] M.S. Jansen, M.U. Christiansen, Effect of Water-solids ratio on the compressive strength and morphology of fly ash-waste glass geopolymer mortars, in: World of Coal Ash (WOCA) Conference, Nasvhille, TN, 2015.
[70] R. Vinai, A. Rafeet, M. Soutsos, W. Sha, The role of water content and paste proportion on physico-mechanical properties of alkali activated fly ash–ggbs concrete, Journal of Sustainable Metallurgy 2 (1) (2016) 51–61.
[71] A. Rafeet, R. Vinai, M. Soutsos, W. Sha, Effects of slag substitution on physical and mechanical properties of fly ash-based alkali activated binders (AABs), Cement Concr. Res. 122 (2019) 118–135.
[72] A. Fernández-Jiménez, F. Puertas, I. Sobrados, J. Sanz, Structure of calcium silicate hydrates formed in alkaline-activated slag: influence of the type of alkaline activator, J. Am. Ceram. Soc. 86 (8) (2003) 1389–1394.
[73] S.K. Lee, J. Stebbins, Disorder and the extent of polymerization in calcium silicate and aluminosilicate glasses: O-17 NMR results and quantum chemical molecular orbital calculations, Geochem. Cosmochim. Acta 70 (16) (2006) 4275–4286.
[74] J.F. Stebbins, Z.J.N. Xu, NMR evidence for excess non-bridging oxygen in an aluminosilicate glass, Nature 390 (6655) (1997) 60–62.
[75] T. Luukkonen, Z. Abdollahnejad, J. Yliniemi, P. Kinnunen, M. Illikainen, One-part alkali-activated materials: a review, Cement Concr. Res. 103 (2018) 21–34.